IEEE Photonics Journal
An IEEE Photonics Society Publication

Open Access

Thermo-Optic Characterization of Silicon Nitride Resonators for Cryogenic Photonic Circuits

Volume 8, Number 3, June 2016

Ali W. Elshaari
Iman Esmaeil Zadeh
Klaus D. Jöns
Val Zwiller

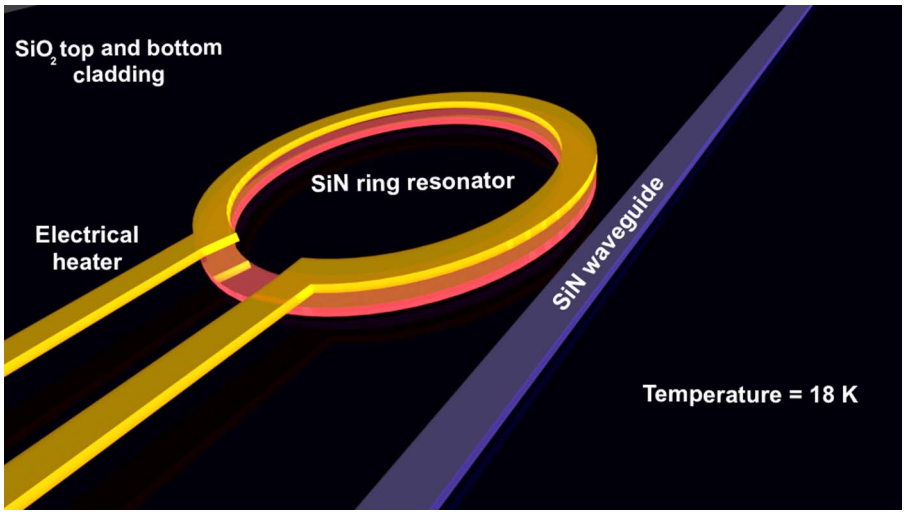

DOI: 10.1109/JPHOT.2016.2561622
1943-0655 © 2016 IEEE

IEEE photonics SOCIETY

IEEE

Thermo-Optic Characterization of Silicon Nitride Resonators for Cryogenic Photonic Circuits

Ali W. Elshaari,[1,2] Iman Esmaeil Zadeh,[1] Klaus D. Jöns,[1,2] and Val Zwiller[2]

[1]Kavli Institute of Nanoscience, Delft University of Technology, 2628 CJ Delft, The Netherlands
[2]Department of Applied Physics, Royal Institute of Technology (KTH), 106 91 Stockholm, Sweden

DOI: 10.1109/JPHOT.2016.2561622
1943-0655 © 2016 IEEE. Translations and content mining are permitted for academic research only. Personal use is also permitted, but republication/redistribution requires IEEE permission. See http://www.ieee.org/publications_standards/publications/rights/index.html for more information.

Manuscript received April 18, 2016; accepted April 28, 2016. Date of publication May 2, 2016; date of current version May 18, 2016. This work was supported in part by the European Union Seventh Framework Program 209 (FP7/2007–2013) under Grant 601126 210 (HANAS) and in part by the Dutch Foundation for Fundamental Research on Matter under FOM-Projectruimte 10NQO02 and FOM-Projectruimte 12PR2994. The work of K. D. Jöns was supported by the MARIE SKLODOWSKA-CURIE Individual Fellowship under REA Grant 661416 (SiPhoN). Corresponding author: A. W. Elshaari (e-mail: elshaari@kth.se).

Abstract: In this paper, we characterize the Thermo-optic properties of silicon nitride ring resonators between 18 and 300 K. The Thermo-optic coefficients of the silicon nitride core and the oxide cladding are measured by studying the temperature dependence of the resonance wavelengths. The resonant modes show low temperature dependence at cryogenic temperatures and higher dependence as the temperature increases. We find the Thermo-optic coefficients of PECVD silicon nitride and silicon oxide to be 2.51 ± 0.08 E-5 K^{-1} and 0.96 ± 0.09 E-5 K^{-1} at room temperature while decreasing by an order of magnitude when cooling to 18 K. To show the effect of variations in the thermo-optic coefficients on device performance, we study the tuning of a fully integrated electrically tunable filter as a function of voltage for different temperatures. The presented results provide new practical guidelines in designing photonic circuits for studying low-temperature optical phenomena.

Index Terms: Integrated optics, ring resonator, optical properties.

1. Introduction

Silicon nitride (SiN) is a complementary metal-oxide semiconductor (CMOS)-compatible material that is well known to the computer chip industry as a dielectric insulator [1]. Over the past few years, it has been one of the main platforms for building integrated photonic circuits. Besides offering CMOS compatibility, it has the advantages of relatively large refractive index contrast with silicon oxide (SiO2) enabling dense and small footprint devices [2], [3]; it has no two-photon absorption in the telecom wavelength range due to its large bandgap [4]; and it offers relatively large thermal/Kerr coefficients at room temperature [5]. These properties, among others, enabled a wide variety of room-temperature applications utilizing linear optical components with low propagation losses [6]; high-Q resonators [7]–[9]; and all-optical signal processing/amplification [10], [11]. Naturally, extensive studies to determine the room-temperature thermo-optic properties of SiN have been conducted. Based on integrated waveguide-technique, the room temperature thermo-optic coefficient SiN was previously reported [5], [12], [13]. Low temperature values of the thermo-optic coefficient were only reported for amorphous SiN down to 80 K using

Fabry-Pèrot measurements [14]. Based on the fitted data, a numerical model was constructed, but unfortunately the model breaks-down below 50 K. While characterization at even lower temperatures is highly desired for on-chip quantum photonic applications, no detailed study of the thermo-optic properties of the material at low temperatures have been performed. The quality of integrated optical components depends on the precision of the refractive index information available. Although the absolute value of the index sets the operation point for the device, any fluctuations in temperature will change the refractive index and hence change the optical properties. These fluctuations in the temperature can play a major role in limiting the accuracy of on-chip interferometric and resonant elements. In addition, when building on-chip cryogenic circuits, the available thermal budget for thermo-optic tuning should be carefully investigated. For these reason it's of prime importance to have knowledge of the thermo-optic coefficient of the constituent materials, dn/dT, at low temperatures. In this work, we measure the thermo-optic coefficient of SiN and SiO_2 between 18 K to 300 K based on integrated circuit approach and test the performance of a fully integrated tunable filter. Integrated optical circuits have been used for photon detection [15], [16], coupling from on-chip emitters [17], [18], entangled photon generation with nonlinear processes [19], [20], and spectrograph calibration [21]. Beside faster carrier dynamics and reduced noise [22], low temperature operation is crucial for many applications such as coupling to super conducting single photon detectors [15], [23]. The thermo-optic coefficient plays an important role in tuning [24] and stabilization [25] of integrated optical circuits. Any deviation of the circuit's designed optical properties when subjected to thermal fluctuations or high power operation is of prime importance and will degrade the overall performance [26].

2. Experiment and Results

We characterize the thermo-optic coefficient of PECVD SiN and SiO_2 based on studying the resonance tuning of traveling-wave mode cavities. The devices were fabricated using a 200 mm bare silicon wafer covered with 3 μm-thick thermal oxide serving as a low index barrier for total internal reflection in the SiN waveguide. Then, 200 nm of SiN was deposited using PECVD at 300 °C, following a similar process reported previously [27] with no post-annealing to keep the process CMOS compatible and also to leave the possibilities open for integration with III-V sources [28] and superconducting detectors. Waveguides and ring resonators are patterned using 100 keV e-beam lithography on 950 K PMMA resist. After developing the resist, features were transferred to the SiN by complete etching of the SiN layer using CHF_3/Ar based reactive ion etching. This was followed by a short O_2 plasma cleaning step. Finally, the chip was cladded with 2 μm PECVD SiO_2 for symmetric mode confinement of both orthogonal modes in the waveguide. The chip design employed a U-shape structure [29] with input and output waveguide separation of 40 μm. This simplifies coupling to/from the side facet of the chip and separates input and output beams spatially. Furthermore, the waveguides were terminated with an inverse taper for efficient coupling and to allow only the fundamental mode to be excited [9], [30]. The taper is adiabatically increased to the main waveguide width of 800 nm. The resonator is designed to have a diameter of 140 μm and gaps of 280 nm separating it from the waveguides. Fig. 1(a) shows a scanning electron microscope (SEM) image of the fabricated device. The chip is then cleaved at the inverse taper region along the wafer crystallographic direction to achieve a smooth facet for enhanced coupling. The experimental setup is shown in Fig. 1(b). It consists of a continuous flow cryostat equipped with a PID controlled heater. The imaging system allows to independently view the top/side of the chip through removable beam splitter BS2 and mirror M2. The side view helps to evaluate the laser spot profile while exciting the waveguide. For the excitation, we use a super continuum laser source equipped with an acoustic-optical tunable filter. We use a half-wave plate and a linear polarizer to control the input-state polarization coupled to the waveguide. Finally, the output beam is directed to a 750 mm spectrometer with 1800 g/mm grating terminated with a CCD. Fig. 2(a) shows the drop port transmission of TM and TE modes. The loaded quality factors of TM and TE modes are 12,400 and 27,000, respectively. For the ring-waveguide gap of 280 nm, the coupling rate of the resonant TE modes to the waveguide is

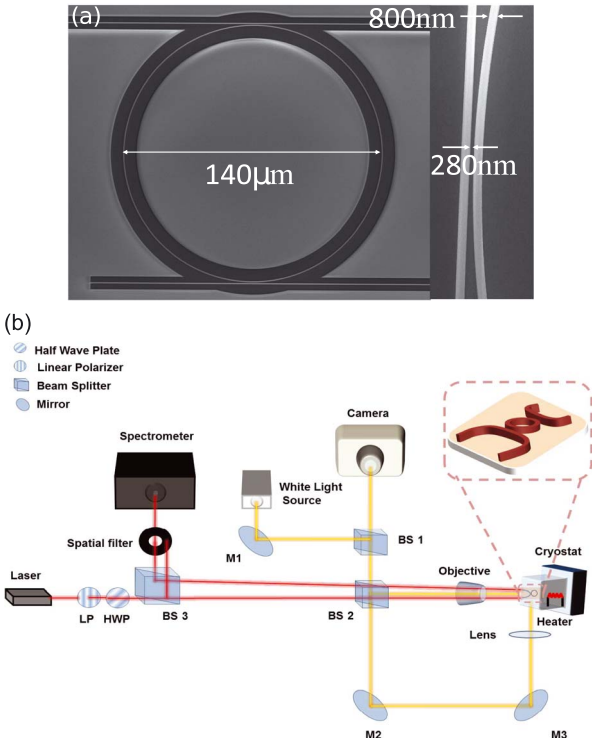

Fig. 1. (a) SEM image of the SiN ring resonator used in the experiment. The resonator has a diameter of 140 μm with waveguide-ring gap of 280 nm. (b) Two-foci experimental setup showing the chip mounted in a continuous-flow cryostat with a local heater. More details are included in the main text.

smaller than the intrinsic cavity loss rate. By measuring the through port transmission for different ring-waveguide gaps, we verify that the TE modes operate in the under-coupled regime, leading to higher loaded Q-values than TM modes at the expense of lower extinction ratio in the through port.

The resonance-wavelength dependence with temperature is studied from 18 K to 300 K. Since in a helium-flow cryostat the sample is cooled from the backside, we investigated if there is any temperature gradient in the sample and deviation in the temperature from the built-in cryostat temperature sensor. For precise sample temperature measurements, we mount a temperature sensor directly on the sample holder. The inset of Fig. 2(c) shows finite element modeling of the temperature distribution in the waveguide region. The simulation shows homogeneous temperature distribution where the optical mode is located while heating is applied to the backside. The sample temperature is modified using the PID controlled heater, while measuring the transmission spectra of TM and TE modes. Fig. 2(b) shows the case of tuning different TM longitudinal resonant modes. We analyzed four resonances for each orthogonal waveguide mode between 850 nm and 880 nm as a function of temperature. The relative resonance shift is extracted then averaged over all four resonances to minimize the measurement errors as shown in Fig. 2(c).

The resonance shifts are measured with respect to the resonant wavelength at 18 K for both orthogonal modes. To ensure high accuracy and thermal stability, each point in the measurement was taken after 30 min from setting the temperature. No thermal fluctuations were observed during data acquisition. From the data we observe that the rate of change in resonance shift increases with temperature, suggesting a deviation from the simple linear dependence around room temperature [31]. The two orthogonal modes tune differently with temperature due to the different confinement factors of the TE and TM modes in the SiN. TM modes extend more

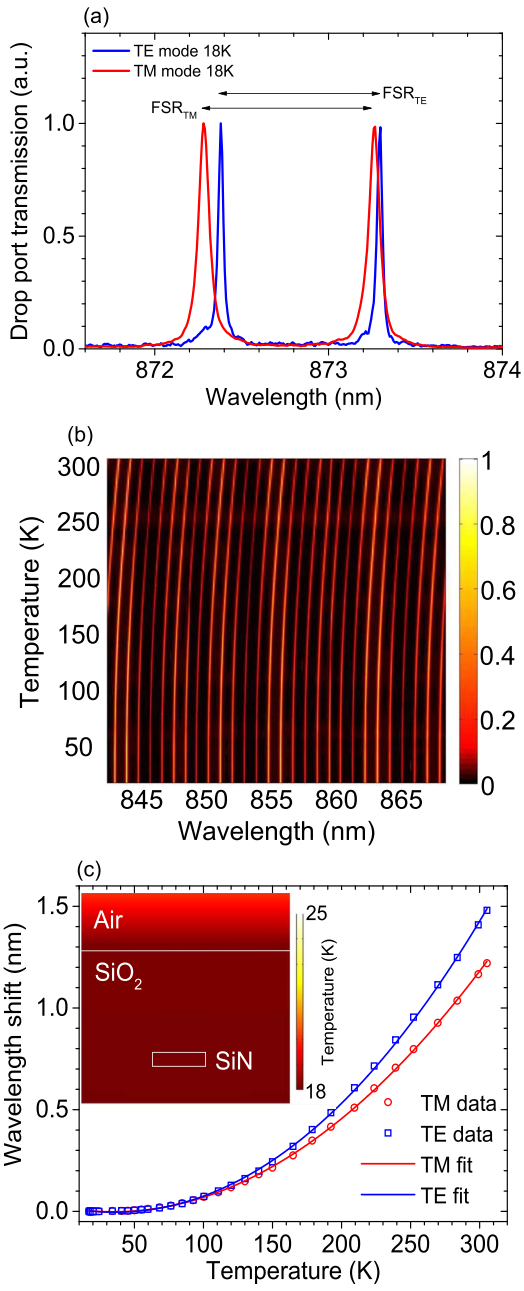

Fig. 2. (a) Drop port transmission for both TE and TM resonant modes. (b) Temperature tuning of TM resonant mode. (c) Resonance shift as a function of temperature. The shifts are measured with respect to resonant wavelengths at 18 K. (Inset) Finite-element method simulation for the temperature distribution at the waveguide.

into the SiO_2 cladding, which has a lower thermo-optic coefficient than the SiN core. Additionally, we performed waveguide loss measurements at room temperature and at 18 K. The losses for TE and TM modes are 4 dB and 2.5 dB, respectively, with no measurable temperature dependence. We attribute this to the dominance of the geometrical waveguide loss due to side wall roughness over the inherent material loss. In order to analyze the data and extract the thermo-optic coefficients of the core and cladding, following the approach presented in [12], we first extract the group index of each guiding mode. The group indexes of TM and TE modes are calculated from

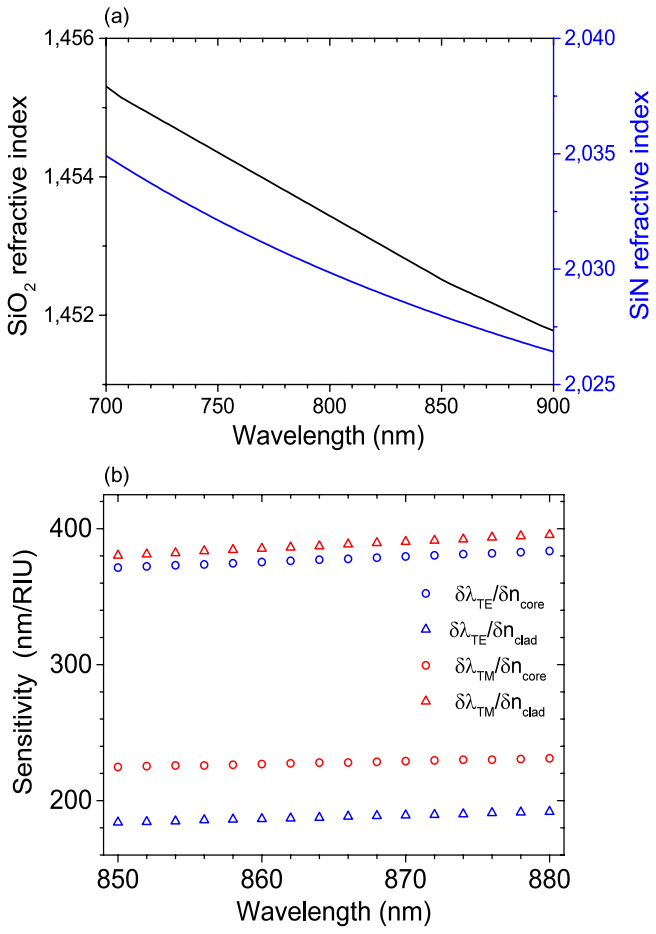

Fig. 3. (a) Ellipsometry measurement of the refractive index of the core and cladding at room temperature. (b) Calculated resonance sensitivity to variations in the core and cladding refractive indexes.

the two measured free-spectral-ranges (FSR) and the length of the resonator [32]. For the TM resonance at 873.25 nm and the TE resonance at 873.3 nm, the measured FSRs are 0.98 nm and 0.92 nm, respectively. These correspond to mode which correspond to $n_{g,TM}$ = 1.767 and $n_{g,TE}$ = 1.882. The thermo-optic coefficient of the core and the cladding materials are extracted by relating the thermally induced resonance shifts to individual material changes [12]:

$$\frac{d\lambda_{TE}}{dT} = \frac{\partial \lambda_{TE}}{\partial n_{core}} \frac{\partial n_{core}}{\partial T} + \frac{\partial \lambda_{TE}}{\partial n_{clad}} \frac{\partial n_{clad}}{\partial T} \tag{1}$$

$$\frac{d\lambda_{TM}}{dT} = \frac{\partial \lambda_{TM}}{\partial n_{core}} \frac{\partial n_{core}}{\partial T} + \frac{\partial \lambda_{TM}}{\partial n_{clad}} \frac{\partial n_{clad}}{\partial T}. \tag{2}$$

To solve these coupled equations for the cladding and core thermo-optic coefficient, we initially calculate the accompanying coefficients $\partial\lambda/\partial n$.

In order to model the cavities accurately we have to determine the dimensions and room temperature parameters accurately. We have captured high resolution SEM of the waveguide to model the dimensions correctly. In addition, ellipsometry measurement for the core and cladding have been performed at room temperature as shown in Fig. 3(a). Based on the ellipsometry data, waveguide SEM images, and the measured $n_{g,TM}$ and $n_{g,TE}$, we use a 3-D full-vectorial mode solver to model the fabricated device and calculate the rate of change of resonance wavelength with respect to the cladding and core refractive indexes at each wavelength, as shown in Fig. 3(b).

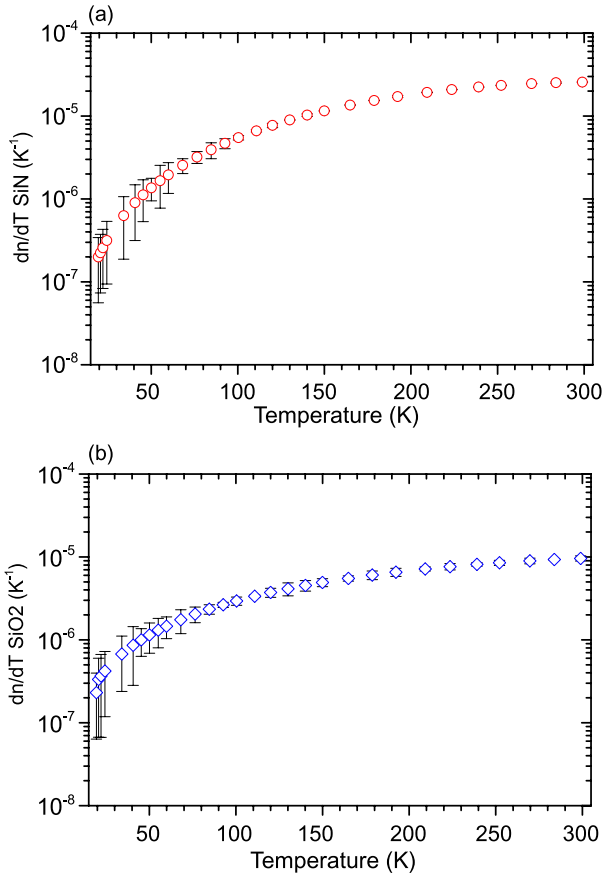

Fig. 4. (a) and (b) Thermo-optic coefficients of SiN and SiO2, respectively, as a function of temperature.

Using this data along with the resonance tuning in Fig. 2(c), we simultaneously solve equations (1) and (2). The results are shown in Fig. 4(a) and (b). The materials thermo-optic coefficients vary by more than 1-order of magnitude between 18 K and 300 K. They approximately plateau near room temperature resulting in a linear response as reported in literature. The measured values at room temperature are $dn_{SiN}/dT \approx (2.51 \pm 0.08) \times 10^{-5}$ K^{-1} $dn_{SiO_2}/dT \approx (0.96 \pm 0.09) \times 10^{-5}$ K^{-1}. These values show excellent agreement with recently reported work [12] with only 2% deviation which is smaller than the measurement errors.

There are different challenges in measuring the refractive index at low temperature. The main difficulty is having good thermal stability in the system. Additionally, a sensitive resonant or interferometric effect is required to sense any changes in the material properties. Compared to previous integrated approaches, the measurement is performed in a continuous flow cryostat under high vacuum to yield the maximum stability and extract the true material properties at each temperature, with minimum dependence on the environment. Another challenge in performing low temperature measurements is extracting the sample temperature accurately which is crucial in measuring the refractive index of both materials. Here, two temperature measurements are performed: one with PID controlled heater/sensor in the continuous flow cryostat, while the second is taken with a high sensitivity low temperature diode mounted directly on the sample holder. For the tolerance values presented in Fig. 4(a) and (b), we performed error propagation to include different types of errors in the measurement. The spectrometer resolution was limited to 0.0076 nm at 1800 g/mm, putting a lower limit on the smallest measurable resonance shift. Temperature measurement error was limited by the accuracy of the voltage reading

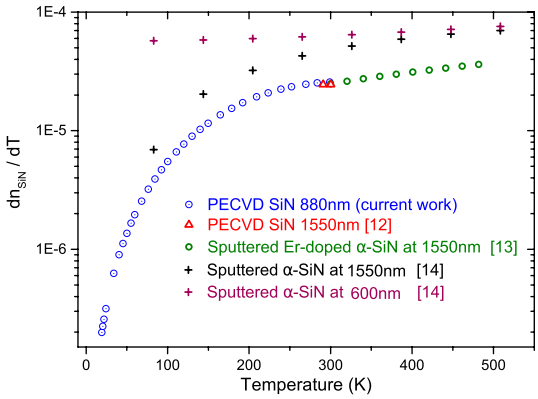

Fig. 5. Thermo-optic coefficient of silicon nitride reported in literature.

on the diode and the corresponding temperature in its response function. Finally, the fitting error is included and propagated through all the numerical operations, which is minimized by tracking multiple resonances and averaging over them. By fitting the measured data, we extract the temperature-dependent thermo-optic coefficients of SiN and SiO^2 for the temperature range investigated.

$$\frac{dn_{\mathrm{SiN}}}{dT}(T) = 3.211 \times 10^{-7} - 1.990 \times 10^{-8} \times T + 8.856 \times 10^{-10} T^2 - 1.375 \times 10^{-12} T^3 - 1.105 \times 10^{-15} T^4 \quad (3)$$

$$\frac{dn_{\mathrm{SiO_2}}}{dT}(T) = -1.167 \times 10^{-7} + 1.727 \times 10^{-8} \times T + 1.861 \times 10^{-10} T^2 - 5.781 \times 10^{-13} T^3 + 4.221 \times 10^{-16} T^4. \quad (4)$$

Fig. 5 shows reported values in literature for the thermo-optic cofficient of silicon nitride at different temperatures and measurement wavelengths. The presented work nicely complements the reported data for room temperature measurements and higher. On the otherhand, we see that the sputtered SiN in [14] provides a slightly higher thermo-optic coefficient at visible and near infra-red range, which may be attributed to different silicon content in the sample, generally, the thermo-optic coefficient depends on the operating wavelength and the material composition. For the presented measurements, we used a silicon nitride deposition process that is similar to the work in [27].

To stress the importance of the presented results for low temperature performance of photonic circuits, we fabricated local heaters on the ring resonators as shown in Fig. 6(a). The heater consists of 80 nm thick titanium resistor separated by 3 micrometer of PECVD SiO_2 from the ring. Although the small misalignment between the resonator and the heater decreases the efficiency of the tuning mechanism, we can compare the tuning power needed to achieve the same wavelength shift for different temperature ranges using the same device. The resonance shift of the TE mode as a function of the heater power is shown in Fig. 6(b). We clearly see larger resonance tuning at room temperature compared to starting the tuning at 18 K due to the larger thermo-optic coefficient. To reduce the required heat-budget, accurate heater-ring alignment in addition to innovative heater designs may be employed, such as the micro-oven approach [33].

3. Conclusion

In summary, we have measured the thermo-optic coefficients of SiN and SiO2 as a function of temperature between 18 K and 300 K. The thermo-optic coefficients change by more than one order of magnitude over the whole temperature range. The SiN resonators have considerably

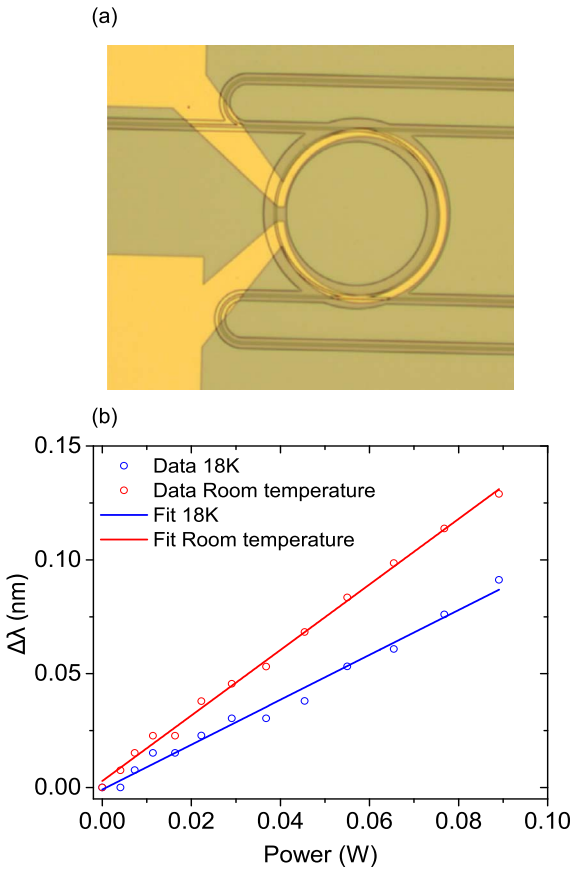

Fig. 6. (a) Microscope image of a top-heater integrated with a SiN ring-resonator. (b) Wavelength shift as a function of the heater power at room temperature (red) and at 18 K (blue).

high thermal stability at low temperatures at the expense of tunability. As an example, we studied the performance of a fully integrated electro-optic filter at 18 K and at room temperature and showed that the filter has considerably smaller tuning range at lower temperatures. As higher temperatures generally degrade the performance of quantum emitters and single photon detectors, the less efficient tuning sets a limit on the available thermal budget in such circuits. The presented results can be used as a reference for future designs of complex integrated photonic cryogenic circuits.

References

[1] D. J. Moss, R. Morandotti, A. L. Gaeta, and M. Lipson, "New CMOS-compatible platforms based on silicon nitride and Hydex for nonlinear optics," *Nat. Photon.*, vol. 7, pp. 1749–4885, 2013.
[2] J. Riemensberger *et al.*, "Dispersion engineering of thick high-*Q* silicon nitride ring-resonators via atomic layer deposition," *Opt. Exp.*, vol. 20, no. 25, pp. 27661–27669, 2011.
[3] M. A. Popovíc *et al.*, "Multistage high-order microring-resonator add-drop filters," *Opt. Lett.*, vol. 31, pp. 2571–2573, 2006.
[4] D. T. H. Tan, K. Ikeda, P. C. Sun, and Y. Fainman, "Group velocity dispersion and self phase modulation in silicon nitride waveguides," *Appl. Phys. Lett.*, vol. 96, vol. 6, 2010, Art. no. 061101.
[5] K. Ikeda, R. E. Saperstein, N. Alic, and Y. Fainman, "Thermal and Kerr nonlinear properties of plasma-deposited silicon nitride/silicon dioxide waveguides," *Appl. Phys. Lett.*, vol. 16, no. 17, pp. 12987–12994, 2008.
[6] J. F. Bauters *et al.*, "Ultra-low-loss high-aspect-ratio Si3N4 waveguides," *Opt. Exp.*, vol. 19, no. 4, pp. 3163–3174, 2011.
[7] A. Griffith, J. Cardenas, C. B. Poitras, and M. Lipson, "High quality factor and high confinement silicon resonators using etchless process," *Opt. Exp.*, vol. 20, pp. 21341–21345, 2012.

[8] Q. Li *et al.*, "Vertical integration of high-*Q* silicon nitride microresonators into silicon-on-insulator platform," *Opt. Exp.*, vol. 21, no. 15, pp. 18236–18248, 2013.
[9] A. Gondarenko, J. S. Levy, and M. Lipson, "High confinement micron-scale silicon nitride high Q ring resonator," *Opt. Exp.*, vol. 17, no. 14, pp. 11366–11370, 2009.
[10] J. S. Levy *et al.*, "CMOS-compatible multiple-wavelength oscillator for on-chip optical interconnects," *Nat. Photon.*, vol. 4, pp. 1749–4885, 2010.
[11] Y. Okawachi *et al.*, "Octave-spanning frequency comb generation in a silicon nitride chip," *Opt. Lett.*, vol. 36, no. 17, pp. 3398–3400, 2011.
[12] A. Arbabi and L. L. Goddard, "Measurements of the refractive indices and thermo-optic coefficients of Si3N4 and SiOx using microring resonances," *Opt. Lett.*, vol. 38, no. 19, pp. 3878–3881, Oct. 2013.
[13] A. C. Hryciw, R. D. Kekatpure, S. Yerci, L. D. Negro, and M. L. Brongersma, "Thermo-optic tuning of erbium-doped amorphous silicon nitride microdisk resonators," *Appl. Phys. Lett.*, vol. 98, no. 4, 2011, Art. no. 041102.
[14] A. R. Zanatta and I. B. Gallo, "The thermo optic coefficient of amorphous SiN films in the near-infrared and visible regions and its experimental determination," *Appl. Phys. Exp.*, vol. 6, no. 4, 2013, Art. no. 042402.
[15] C. Schuck, W. H. P. Pernice, and H. X. Tang, "Waveguide integrated low noise NbTiN nanowire single-photon detectors with milli-Hz dark count rate," *Sci. Rep.*, vol. 3, 2013, Art. no. 1893.
[16] W. H. P. Pernice *et al.*, "High-speed and high-efficiency travelling wave single-photon detectors embedded in nanophotonic circuits," *Nat. Commun.*, vol. 3, 2012, Art. no. 1325.
[17] S. L. Mouradian *et al.*, "Efficient integration of high-purity diamond nanostructures into silicon nitride photonic circuits," in *Proc. CLEO*, 2014, pp. 1–2.
[18] Y. Gong *et al.*, "Linewidth narrowing and Purcell enhancement in photonic crystal cavities on an Er-doped silicon nitride platform," *Opt. Exp.*, vol. 18, no. 3, pp. 2601–2612, 2010.
[19] Y.-P. Huang, V. Velev, and P. Kumar, "Quantum frequency conversion in nonlinear microcavities," *Opt. Lett.*, vol. 38, no. 12, pp. 2119–2121, Jun. 2013.
[20] R. Wakabayashi *et al.*, "Time-bin entangled photon pair generation from Si micro-ring resonator," *Opt. Exp.*, vol. 23, pp. 1103–1113, 2015.
[21] T. J. Kippenberg, R. Holzwarth, and S. A. Diddams, "Microresonator-based optical frequency combs," *Science*, vol. 332, pp. 555–559, 2011.
[22] W. H. P. Pernice, C. Schuck, M. Li, and H. X. Tang, "Carrier and thermal dynamics of silicon photonic resonators at cryogenic temperatures," *Opt. Exp.*, vol. 19, pp. 3290–3296, 2011.
[23] M. K. Akhlaghi, E. Schelew, and J. F. Young, "Waveguide integrated superconducting single-photon detectors implemented as near-perfect absorbers of coherent radiation," *Nat. Commun.*, vol. 6, p. 9233, Sep. 2015.
[24] R. Amatya, C. W. Holzwarth, H. I. Smith, and R. J. Ram, "Precision tunable silicon compatible microring filters," *IEEE Photon. Technol. Lett.*, vol. 20, no. 20, pp. 1739–1741, Oct. 2008.
[25] S. Yokoyama, F. Qiu, Y. Feng, A. M. Spring, and K. Yamamoto, "0.018 pm/°C athermal silicon nitride ring resonator by polymer cladding," in *Proc. CLEO-PR*, 2013, pp. 1–2.
[26] B. Guha, J. Cardenas, and M. Lipson, "Athermal silicon microring resonators with titanium oxide cladding," *Opt. Exp.*, vol. 21, no. 22, pp. 26557–26563, 2013.
[27] A. Gorin, A. Jaouad, E. Grondin, V. Aimez, and P. Charette, "Fabrication of silicon nitride waveguides for visible-light using PECVD: A study of the effect of plasma frequency on optical properties," *Opt. Exp.*, vol. 16, no. 18, pp. 13509–13516, 2008.
[28] I. Esmaeilzadeh *et al.*, "Deterministic integration of single photon sources in silicon based photonic circuits," *Nano Lett.*, vol. 16, pp. 2289–2294, 2016.
[29] Y. Xia, C. Qiu, X. Zhang, W. Gao, J. Shu, and Q. Xu, "Suspended Si ring resonator for mid-IR application," *Opt. Lett.*, vol. 38, no. 7, pp. 1122–1124, 2013.
[30] A. C. Turner *et al.*, "Tailored anomalous group-velocity dispersion in silicon channel waveguides," *Opt. Exp.*, vol. 14, pp. 4357–4362, 2006.
[31] N. Ter-Gabrielyan, V. Fromzel, and M. Dubinskii, "Linear thermal expansion and thermo-optic coefficients of YVO4 crystals the 80–320 K temperature range," *Opt. Exp.*, vol. 2, pp. 1624–1631, 2012.
[32] P. Rabiei, W. H. Steier, C. Zhang, and L. R. Dalton, "Polymer micro-ring filters and modulators," *J. Lightw. Technol.*, vol. 20, no. 11, pp. 1968–1975, Nov. 2002.
[33] L. Cao, A. A. Aboketaf, and S. F. Preble, "CMOS compatible micro-oven heater for efficient thermal control of silicon photonic devices," *Opt. Commun.*, vol. 305, pp. 66–70, Sep. 2013.